Eur. Phys. J. A (2024) 60:122
https://doi.org/10.1140/epja/s10050-024-01342-2

THE EUROPEAN
PHYSICAL JOURNAL A

Regular Article - Experimental Physics

Elastic and inelastic scattering measurements for the ^{13}C+^{208}Pb system at close to the Coulomb barrier energies

P. L. D. Magro[1], **V. Guimarães**[1,a], **M. Assunção**[2], **E. O. N. Zevallos**[1,3], **M. B. Angelo**[1], **L. M. Garcia-Figueroa**[1], **F. Miletto**[1], **A. Arazi**[4,5], **D. Hojman**[4,5], **M. A. Cardona**[4,5] , **E. de Barbará**[4], **J. Gomez**[4,5], **B. Paes**[4,5], **E. N. Cardozo**[6], **J. Lubian**[6], **J. C. Zamora**[7]

[1] Instituto de Física, Universidade de São Paulo, Rua do Matão 1371, São Paulo, SP 05508-090, Brazil
[2] Departamento de Física, Universidade Federal de São Paulo, Campus Diadema, São Paulo 09913-030, Brazil
[3] Universidad Científica del Sur, Lima 15067, Peru
[4] Laboratorio TANDAR, Comisión Nacional de Energía Atómica, Buenos Aires, BKNA 1650, Argentina
[5] Consejo Nacional de Investigaciones Científicas y Técnicas, Buenos Aires C1425FQB, Argentina
[6] Instituto de Física, Universidade Federal Fluminense, Avenida Litoranea s/n, Gragoatá, Niterói, RJ 24210-340, Brazil
[7] Facility for Rare Isotope Beams, Michigan State University, East Lansing, MI 48824, USA

Received: 12 February 2024 / Accepted: 19 May 2024 / Published online: 10 June 2024

Communicated by Alessia Di Pietro

Abstract Angular distributions for elastic and inelastic scattering of the ^{13}C+^{208}Pb system have been measured at energies close to the Coulomb barrier, E_{lab} = 59.8, 63.8 and 65.8 MeV. Optical Model (OM) and coupled channel (CC) analysis were performed using Woods-Saxon and double folding São Paulo potentials. Angular distributions for the $J^{\pi} = 3/2^{-}$ excited state of ^{13}C* (3.684 MeV) and $J^{\pi} = 3^{-}$ of ^{208}Pb* (2.615 MeV) were also obtained and analyzed with coupled channels calculations. A good description of the elastic angular distributions was achieved with the inclusion of the $1n$-stripping contribution in the coupled reaction channel (CRC) calculations.

1 Introduction

Although elastic scattering is the simplest two-body interaction process in a nuclear collision, it can be used to extract information on the dynamics and structures of the involved nuclei [1]. Owing to its peripheral nature, this process has been used to investigate surface and cluster effects of weakly-bound and exotic nuclei [2,3]. For stable and not so deformed projectile on heavy targets, the elastic scattering cross section typically follows a Rutherford cross section at very forward angles ($\sigma_{el}/\sigma_{Ruth} \approx 1$), followed by an oscillatory pattern due to the interference of Coulomb and nuclear scattering, resulting in a Fresnel peak [1]. The strong fall of the cross sections at backward angles represents the absorption effects of the elastic flux by other channels such as fusion and direct reactions (inelastic excitations, transfer, and breakup). Strong coupling effects, arising from deformation of the colliding nuclei or absorption from different channels, can have a significant impact in the elastic scattering angular distributions behavior, which provides an effective mean to probe specific nuclear structure properties of the projectile or target, or the importance of the coupling to a specific channel (dynamic effects) [1,4]. For instance, inelastic scattering is an important channel for deformed projectile, whereas breakup and/or transfer are the important channels for weakly-bound nuclei. Deformation, unusual density distribution, strong cluster structure of the projectile and/or target can also play an important role in modifying the elastic scattering angular distribution, for instance, by deviating the elastic flux from the forward to backward angles due to coupling to other channels (static effect). Also, for weakly-bound projectile on a heavy target, the Fresnel peak in the angular distributions can be completely damped due to the Coulomb field of a heavy target and possible long-range component of the nuclear potential. A review on these effects in the elastic scattering can be found in Ref. [5].

The dynamic and static effects discussed above have been observed in the elastic scattering of different carbon isotopes projectiles on heavy targets. For instance, elastic-scattering angular distributions of the proton-rich ^{9}C [6] and ^{10}C [7] isotopes, as well as for ^{11}C [7], ^{12}C [8], ^{13}C [9,10] and ^{14}C [10] on ^{208}Pb target have been measured at three to five times the Coulomb barrier. The obtained angular distributions for all these experiments present a clear Fresnel peak and do not

---

[a] e-mail: valdirg@if.usp.br (corresponding author)

present any strong coupling effects. On one hand, the relative high velocity of the projectile may prevent any strong interaction with the target. But, on the other hand, at energies close to the Coulomb barrier, strong coupling effects, and damping of the Fresnel peak, are present in the elastic data for the proton-rich ^{10}C isotope on ^{208}Pb [11] and for the very neutron-rich ^{15}C isotope on ^{208}Pb [12]. While for ^{10}C the effects are attributed to the strong cluster structure of this brunnian nucleus ($\alpha + \alpha + p + p$), for ^{15}C it is due to the low valence neutron separation energy (S_n = 1.218 MeV), corresponding to the ^{14}C+n configuration. Although ^{12}C is a deformed (and tightly bound) nucleus, the angular distributions of the elastic scattering on ^{208}Pb [13], measured at energies close to the barrier, do not exhibit any strong absorption effect. To complete the systematic of elastic scattering measurements for the carbon isotopes on a ^{208}Pb target, at energies close to the barrier, data for four projectiles are missing: ^{9}C, ^{11}C, ^{13}C and ^{14}C. In the present work we report, for the first time, elastic scattering data for ^{13}C on ^{208}Pb system at the energies near the Coulomb barrier. Additionally, angular distributions for the excited states at 3.684 MeV in ^{13}C ($3/2^-$) and 2.615 MeV in ^{208}Pb (3^-) have been measured and are included in the present analysis. The measured angular distributions were analyzed with Optical Model (OM), coupled-channel (CC) calculations, where projectile and target inelastic channels were included in the coupling matrix, and coupled-reaction channels (CRC) calculation for the 1n-stripping reaction.

The present paper is organized as follows: in Sect. 1 we provide details of the experiment. In Sect. 2, the analysis of elastic and inelastic angular distributions and the corresponding discussions are presented. The conclusions are given in Sect. 3.

2 Experimental setup

The experiment was performed at Tandar Laboratory of the Comisión Nacional de Energía Atómica, in Buenos Aires, Argentina. The $^{13}C^{6+}$ ion beam was delivered by the 20-UD tandem accelerator at three energies: E_{lab} = 60, 64 and 66 MeV. The ^{13}C beam was impinged on a ^{208}Pb target, 350 μg/cm^2 thick, positioned on a rotating target holder at the center of the scattering chamber. The target was rotated by 40° relative to the beam axis. The energies of the ^{13}C projectile at the center of the target were 59.8, 63.8 and 65.8 MeV, respectively. The Coulomb barrier was estimated to be V_B = 57.3 MeV for this system with the São Paulo potential (SPP2) [14].

The detection system consisted of an array of eight single silicon surface barrier detectors, with an angular separation of 5° between adjacent detectors, referred here as $Z8$. This system has been used in several other elastic scattering measurements with good results [15–17]. An additional silicon planar barrier detector, denominated as *monitor*, was fixed at $\theta_{lab} = 16.1°$. The measurement of the cross section at this angle was used for normalization purposes, since it is pure Rutherford at the energies under consideration.

The yields for elastic and inelastic scattering for each measured angle were obtained by integrating the corresponding peaks in the calibrated energy spectra for each detector in the $Z8$ system. These detectors were calibrated using the elastic scattering data obtained for the ^{16}O+^{197}Au and ^{16}O+^{208}Pb systems at E_{lab} = 25 and 50 MeV, respectively. The elastic scattering at forward angles was assumed to be purely Rutherford. A typical energy spectrum measured for ^{13}C+^{208}Pb at $\theta_{lab} = 55.0°$ can be seen in Fig. 1. The energy resolution, derived from the elastic peak, varied from 350 keV (FHWM) at forward angles to 700 keV (FHWM) for the spectra measured at more backward angles, mainly due to the straggling of energy in the target. The elastic and two excited states peaks, at 3.684 MeV (^{13}C*) and 2.615 MeV (^{208}Pb*), can be clearly seen and separated. Angular distributions were measured in the range θ_{lab} = 30.0° to 155.0° with an estimated angular resolution varying between 0.2° and 0.7°. Using the yields from the monitor detector, the cross sections for each measured angle, normalized to Rutherford cross section, were straightforwardly determined according to the expression below:

$$\frac{\sigma}{\sigma_{ruth}}(\theta^i_{cm}) = \frac{\sigma_{ruth}(\theta^{mon}_{cm})}{\sigma_{ruth}(\theta^i_{cm})} \frac{\Delta\Omega_{mon}}{\Delta\Omega^i_{det}} \frac{N^i_{det}}{N_{mon}} \frac{J(\theta^i_{cm})}{J(\theta^{mon}_{cm})}, \qquad (1)$$

where N^i_{det} and N_{mon} are the elastic yields obtained in the detector i and in the monitor, $J(\theta^i_{cm})$ and $J(\theta^{mon}_{cm})$ are the Jacobian of coordinate transformation for the laboratory to center of mass system. $\sigma_{ruth}(\theta^i_{cm})$ and $\sigma_{ruth}(\theta^{mon}_{cm})$ are the differential elastic cross sections at θ^i_{cm} and θ^{mon}_{cm}, respec-

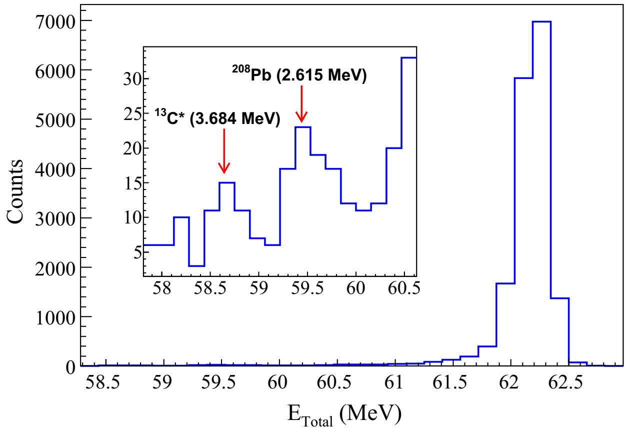

Fig. 1 Energy spectrum for ^{13}C+^{208}Pb measured at E_{lab} = 65.8 MeV and θ_{lab} = 55.0°. The small peaks corresponding to the excited state of ^{13}C ($3/2^-$) and ^{208}Pb (3^-) are also indicated

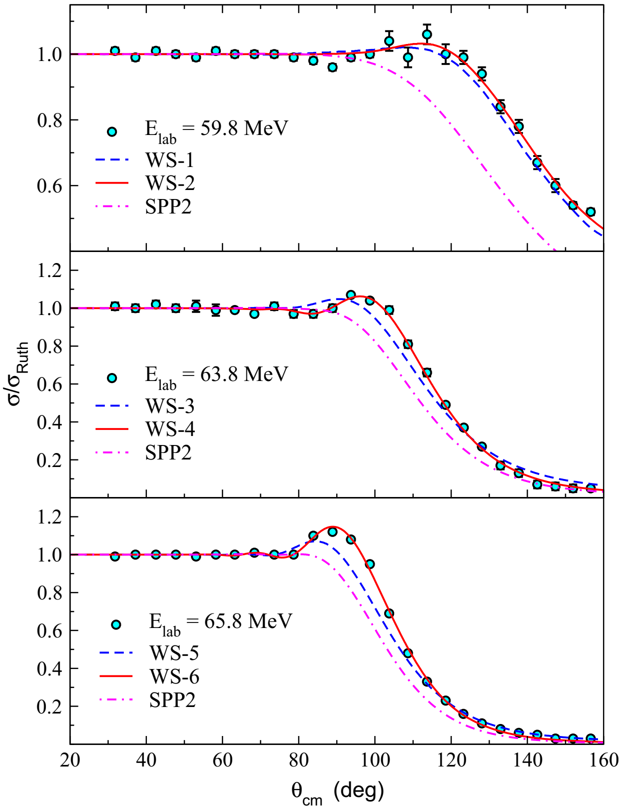

Fig. 2 Elastic scattering angular distribution for the ^{13}C+^{208}Pb at E$_{lab}$ = 59.8, 63.8 and 65.8 MeV. The solid and dashed curves are OM calculations with WS potential with the parameters listed in Table 1. The dashed-dotted curve represents the OM calculation with the SPP2 potential with normalization N_R = 1.0 and N_I = 0.78 for real and imaginary parts, respectively

tively. The $\Delta\Omega_{mon}/\Delta\Omega^{i}_{det}$ solid angle ratio was obtained from the analysis of the ^{16}O+^{197}Au elastic scattering data, measured in the same experiment at E$_{lab}$ = 25.0 MeV, which corresponds to an energy well below the Coulomb barrier where the cross sections, at all angles, were purely Rutherford.

3 Analysis

3.1 Optical model

The experimental angular distributions for the elastic scattering of the ^{13}C+^{208}Pb system are shown in Fig. 2 for E_{lab} = 59.8, 63.8 and 65.8 MeV, respectively. The error bars of the differential cross sections were estimated considering only statistical uncertainties. Using the yields of the monitor detector, the contributions from number of particles in the beam and number of particles in the target are canceled out. The systematic uncertainty comes only from the ratio of the solid angles between each detector and the fixed monitor detector and are in the range of 1–10%. In the plots only statistical uncertainties are computed, and they are in the range of 1–3% (10% for the most backward angles). It is important to note that the Fresnel-like diffraction pattern is observed in the angular distribution measured at E_{lab} = 65.8 MeV and 63.8 MeV. However, for the angular distribution at the energy closer to the barrier, E_{lab} = 59.8 MeV, the Fresnel peak is practically absent. Optical model (OM) calculations were performed for these angular distributions considering both a volume type Woods-Saxon (WS) and a double folding potential. Parameters for the WS potentials are listed in Table 1. The WS-1, WS-3 and WS-5 were taken from the analysis of the ^{12}C+^{208}Pb data at E$_{lab}$ = 60.9 MeV (WS-1) and 64.9 MeV (WS-3 and WS-5) as reported in Ref. [18] and used to calculate the cross sections for ^{13}C+^{208}Pb. As can be observed in Fig. 2, these potentials do not provide a good description of the experimental angular distributions. Therefore, a fitting procedure was, then, performed to search for the optimal parameters for the depths, radii and diffuseness of the real and imaginary parts, using as the initial parameters those from the previous potentials. The obtained parameters, which minimize the χ^2 of the fitting, are given by WS-2 (E_{lab} = 59.8 MeV), WS-4 (E_{lab} = 64.8 MeV) and WS-6 (E_{lab} = 65.9 MeV) in Table 1. The fitting of the angular distributions with these potentials are quite good for all three measured energies. The important point for this analysis is to derive the total reaction cross sections (σ_R). The values obtained for the ^{13}C+^{208}Pb using the WS-2, WS-4 and WS-6 are listed in Table 1. The uncertainty in the total reaction cross section was estimated by considering the beam energy resolution (0.5 MeV) in the fitting procedure.

For comparison, we have plotted the angular distributions for the elastic scattering obtained in this work for ^{13}C at E$_{lab}$ = 65.8 MeV along with those obtained for other carbon isotopes as projectile, at similar energies, ^{10}C at E$_{lab}$ = 66 MeV [11], ^{12}C at E$_{lab}$ = 64.9 MeV [13] and ^{15}C at E$_{lab}$ = 65 MeV [12] on ^{208}Pb target, see Fig. 3. The energies for all these systems are slightly above the corresponding Coulomb barrier. Besides the different isospin asymmetry, the carbon isotopes projectiles have different particle separation energies: ^{10}C (S$_p$ = 4.006 MeV), ^{12}C (S$_\alpha$ = 7.367 MeV), ^{13}C (S$_n$ = 4.946 MeV), and ^{15}C (S$_n$ = 1.218 MeV). As can be observed in the figure, the Fresnel-like pattern is pronounced for the stable isotopes ^{12}C and ^{13}C, but strongly damped for ^{10}C and ^{15}C. The curves in the figure are OM calculations, using parameters from WS potentials obtained in the respective references. Actually, for both ^{10}C and ^{15}C projectiles, the cross section at backward angles are strongly absorbed. For the proton-rich ^{10}C, this absorption was attributed by Linares et al. to its *Brunnian* structure [11], while for the neutron-rich ^{15}C isotope it was attributed to the unique s-wave nature of the halo wave function in ^{15}C [12], but with the caveat that the data was still at the preliminary stage. For a further

Table 1 Parameters of the potentials used in Optical Model analysis

Energy	Potential	V	r_V	a_V	W	r_W	a_W	σ_R (mb)	χ^2_{red}
	WS-1	55.64	1.282	0.483	56.49	1.261	0.384		3.33
E_{lab} = 59.8 MeV	WS-2	50.63	1.347	0.338	40.38	1.177	0.399	87 ± 5	0.92
	WS-3	65.50	1.282	0.463	163.71	1.265	0.365		8.73
E_{lab} = 63.8 MeV	WS-4	45.00	1.307	0.443	140.48	1.212	0.400	381 ± 7	1.18
	WS-5	65.50	1.282	0.463	163.71	1.265	0.365		28.42
E_{lab} = 65.8 MeV	WS-6	68.04	1.279	0.451	140.97	1.226	0.341	442 ± 7	1.33

Parameters for V and W are in MeV. The r_V and r_W are reduced radii in fm, where the radii are obtained using the convention $R_i = r_i \times [A_p^{1/3} + A_t^{1/3}]$ expression. The reduced Coulomb radius is r_C = 1.06 fm. The a_V and a_W are the diffuseness, in fm. The χ^2_{red} is the reduced χ^2. The reaction cross sections (σ_R) obtained with fitted optical potential are also reported with their respective uncertainties

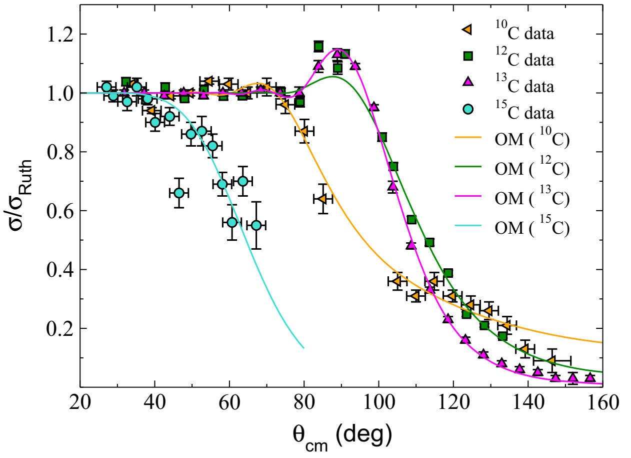

Fig. 3 Elastic scattering angular distributions for the carbon isotopes, ^{10}C at E_{lab} = 66.0 MeV [11], ^{12}C at E_{lab} = 64.9 MeV [13], ^{15}C at E_{lab} = 65 MeV [12] and ^{13}C at E_{lab} = 65.8 MeV on ^{208}Pb target. The OM calculations were performed considering the WS potentials from the respective references

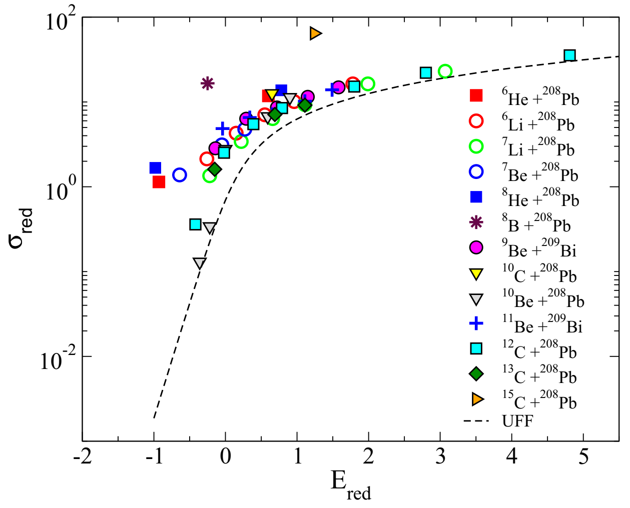

Fig. 4 Reduced total reaction cross section as a function of reduced energy for some light projectiles on heavy target, using the reduction method described in the text. The dashed line curve represents the Universal Fusion Function (UFF), indicating the fusion limit

discussion and to gain some insights on these issues, we can also compare the total reaction cross sections for different projectiles on ^{208}Pb target. However, a proper comparison demands a reduction method to remove differences arising from the static properties and charges of the colliding nuclei. In this work we adopt the reaction function method [19,20], in which the reduced energy (E_{Red}) and the reduced reaction cross section (σ_{Red}) are defined as:

$$E_{\text{red}} = \frac{E_{\text{c.m.}} - V_b}{\hbar\omega}; \qquad \sigma_{\text{red}} = \sigma_R \left[\frac{2E_{\text{c.m.}}}{\hbar\omega R_b^2}\right], \tag{2}$$

where R_b, V_b and $\hbar\omega$ are the radius, height, and width of an inverted parabolic shape adjusted to the Coulomb barrier. The parameters of the Coulomb barrier were determined adopting the São Paulo potential [21] as the nuclear potential and no centrifugal term ($\ell = 0$).

A comparison of the σ_{red} for several light projectiles on ^{208}Pb (and two on ^{209}Bi) target is shown in Fig. 4. At low energy regime, the total reaction cross section should contain a strong contribution of fusion and some contribution from other non-elastic direct reactions such as inelastic, transfer, and breakup cross sections. The fusion contribution can be approximately estimated by considering Wong's model [22], which describes the penetration probability through a fixed parabolic barrier. When considering the present reduced variables, Wong's equation transforms itself into an equation known as the universal fusion function (UFF) [23], which depends only on the reduced energy and therefore, is system independent and it is given by:

$$\sigma_{\text{UFF}} = \ln\left[1 + \exp(2\pi E_{\text{red}})\right] \tag{3}$$

The σ_{UFF} can thus be considered as a lower limit for the σ_{red} due to fusion and the contribution of the several direct reactions to the total reaction can be estimated from the difference $\varDelta = \sigma_{\text{red}} - \sigma_{\text{UFF}}$. A possible correlation between this difference and the separation energy of the valence particles, can be observed in the figure, where higher values are obtained for weakly bound projectiles, suggesting the importance of the breakup process to the total reaction cross section. For instance, the σ_{red} values for ^{8}B and ^{15}C, with S$_p$ = 0.138 MeV and S$_n$ = 1.218 MeV, respectively, are well above the UFF curve. The σ_{red} for some other neutron-rich projectiles, such as ^{6,8}He and ^{11}Be, are also well above the UFF curve. These large total reaction cross sections has been related to the importance of the breakup channel. For tightly bound projectile, as ^{10}Be and ^{12}C, with S$_n$ = 6.812 MeV and S$_\alpha$ = 7.367 MeV, respectively, the reduced total reaction cross sections are closed to the UFF curve. For our ^{13}C+^{208}Pb system, with S$_n$ = 4.946 MeV for ^{13}C, the cross sections follow the trend of the ^{12}C, which is considered a deformed nucleus, indicating that direct channel might have some importance but not as pronounced as for the weakly bound ^{6}He, ^{8}He, ^{8}B, ^{11}Be and ^{15}C projectiles to the total reaction cross section.

OM analysis was also performed by employing the double folding São Paulo (SPP2) nuclear potential [14]. This new version of the São Paulo Potential takes into account the density of the projectile, which can be obtained from a table with experimental charge density values from electron scattering experiments or by nuclear densities calculated with Dirac-Hartree-Bogoliubov model. Additionally, it also includes a dependence on the relative velocity between the colliding nuclei. These features are quite important for radioactive projectiles with nucleus away from the valley-of-stability. Considering the standard real and imaginary normalization factors $N_R = 1.0$ and $N_I = 0.78$, respectively [24], the obtained results for ^{13}C+^{208}Pb are shown in Fig. 2. As can be observed in the figure, the results with SPP2 do not give a good description of the experimental data. However, it is important to mention that this potential could give a good description to the data for the elastic scattering of ^{13}C+^{208}Pb at E_{lab} = 340 MeV [10]. This potential, with the standard normalization parameters (N$_R$ = 1.0 and N$_I$ = 0.78), has been used as benchmark. Deviation of the description of the angular distribution with this potential indicates the importance of other channels, such as inelastic, transfer and breakup, to the elastic scattering. These effects are explored in the next sections, where the results including the couplings of inelastic scattering (CC) and 1n-transfer (CRC) reaction channels are presented.

3.2 Coupling to collective states

To investigate the effect of other channels on the elastic scattering angular distribution for the ^{13}C+^{208}Pb system, we started with the inclusion of the inelastic scattering contributions by performing coupled channel calculations. In this approach, the absorption of the elastic flux is produced by the inelastic excitation of the projectile and/or target nuclei. To account for the absorption due to the fusion reaction, a complex potential was considered, which comprises the SPP2 potential (with N$_R$ = 1.0) as the real part and a short-range Woods-Saxon type potential (W = 50.0 MeV, r$_w$ = 1.06 fm and a$_w$ = 0.2 fm) for the imaginary part [25]. It is important to mention that this short range imaginary potential provides an effective ingoing wave boundary condition for fusion and ensures that any surface absorption was due entirely to the couplings. Also, this short range Woods-Saxon potential has been used with success in several other works [26,27]. In the coupling scheme, we considered the influence of the projectile and the target excitation. For ^{13}C, besides the J$^\pi$ $= 1/2^-$ ground-state, we included in the coupling scheme three excited states at 3.089 MeV (J$^\pi$ $= 1/2^+$), 3.684 MeV (J$^\pi$ $= 3/2^-$) and 3.854 MeV (J$^\pi$ $= 5/2^+$). However, the negative parity state (J$^\pi$ $= 3/2^-$) is expected to give the most relevant contribution, as shown in the work of Barbadoro et al. [28]. For the ^{208}Pb target, besides the J$^\pi$ $= 0^+$ ground-state, the excited states at 2.615 MeV (J$^\pi$ $= 3^-$), and 4.086 MeV (J$^\pi$ $= 2^+$) were considered, since they produce quadrupole and octupole transitions to the ground-state. An extra excited state of ^{208}Pb at 3.198 MeV (J$^\pi$ $= 5^-$) was also included in the coupling scheme. The transitions between the collective states of the projectile and target were described using a model-independent approach, taking into account for each state the corresponding electromagnetic transition $B(E\lambda)$ for both Coulomb and nuclear deformations. The spin, parity, energy of all these states, as well as the values for $B(E\lambda)$, were taken from NNDC database [29] and listed in Table 2. The deformation parameters in Table 2 were calculated from the values of $B(E\lambda)$ using equations from Ref. [30].

Table 2 Deformation parameters of the excited states of the ^{13}C projectile and the ^{208}Pb target used in the calculations

	States of ^{13}C			
E (MeV)	$J_i^\pi \to J_f^\pi$	λ	$B(E\lambda)$ $[W.u]$	δ [fm]
3.089	$1/2^+ \rightleftharpoons 1/2^-$	1	0.039 (4)	0.116
3.684	$3/2^- \rightleftharpoons 1/2^-$	2	3.5 (8)	1.412
	$3/2^- \rightleftharpoons 1/2^+$	1	0.039 (6)	0.1646
3.854	$5/2^+ \rightleftharpoons 1/2^-$	3	10 (4)	2.758
	$5/2^+ \rightleftharpoons 1/2^+$	2	1.65 (7)	1.188
	States of ^{208}Pb			
E (MeV)	$J_i^\pi \to J_f^\pi$	λ	$B(E\lambda)$ $(W.u)$	δ
2.615	$3^- \rightleftharpoons 0^+$	3	33.8 (6)	1.010
3.198	$5^- \rightleftharpoons 3^-$	2	0.39 (2)	0.143
4.086	$2^+ \rightleftharpoons 0^+$	2	8.4 (5)	0.451

Here δ is the deformation length used as input in the FRESCO code

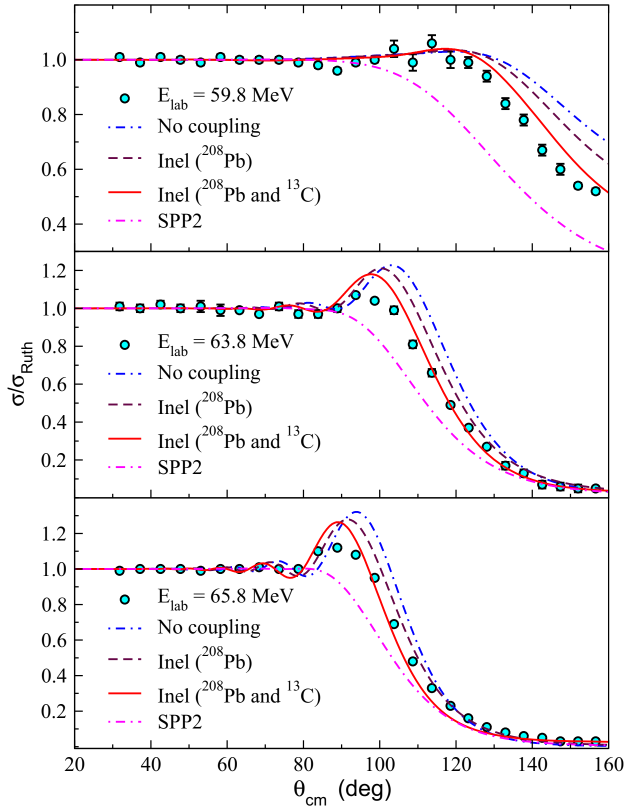

Fig. 5 Elastic scattering angular distribution for the ^{13}C+^{208}Pb at E_{lab} = 59.8, 63.8 and 65.8 MeV. The red solid curve are CC calculations. The blue dashed-dotted curve represents the calculations without the couplings. The magenta dashed-dotted curve represents the OM calculation for SPP2 potential with normalization set to $N_R = 1.0$ and $N_I = 0.78$ for real and imaginary parts, respectively

The results of the CC calculation, carried out using the code FRESCO [31], are shown in Fig. 5. For comparison, we also present the no-coupling calculations (considering only the absorption due to the fusion channel), and the previous results from OM analysis with the SPP2 potential. As observed in the figure, the inelastic coupling improves the description of the data when compared to the no-coupling calculations, being the contribution of the ^{13}C excitation slightly more relevant than the ^{208}Pb excitations. The effect of the coupling to these inelastic channels in the elastic angular distribution measured at E_{lab} = 63.8 and 65.8 MeV is to reduce the intensity and shift the Fresnel peak to smaller angles. Also, for all measured angular distributions there is a reduction of the elastic cross sections at backward angles, compared to the no-coupling calculations.

In the present work, the inelastic cross sections for the excited state of ^{13}C at 3.684 MeV ($J^{\pi} = 3/2^{-}$) and of ^{208}Pb at 2.615 MeV ($J^{\pi} = 3^{-}$) were also measured. The angular distributions for these inelastic channels are displayed in Fig. 6, including the results of the CC calculations for the respective excited states. The peak corresponding to the inelastic scattering populating the first excited state of ^{208}Pb at 2.615 MeV is well separated from the elastic and other excited states, as can be seen in Fig. 1. However, the second peak in the spectrum, corresponding to the excited state at 3.684 MeV ($J^{\pi} = 3/2^{-}$) in ^{13}C, although strong at forward angles, it has some contribution from the other excited states from both ^{13}C and ^{208}Pb at backward angles, where the energy resolution is worse. It should be mentioned that the inelastic cross sections for the ^{208}Pb excited states, 3.475 (4^{-}), 3.708 (5^{-}), 3.919 (6^{-}), 3.947(4^{-}) and 3.961 (5^{-}), are found to be small by our CC calculations. However, a contribution of these states to the 3.684 MeV peak can not be ruled out at backward angles. As can be seen in the figure, the CC calculations agrees fairly well with the data at forward angles for both inelastic states. This can be considered a good achievement since this is a parameter-free calculation. The important point is that the calculations provide a reliable estimate of the intensity of the main nonelastic channels, validating the CC calculations for the elastic channel. Although the inclusion of the nonelastic process in the coupling scheme had quite an impact in the description of the elastic data, there is still room for further improvement.

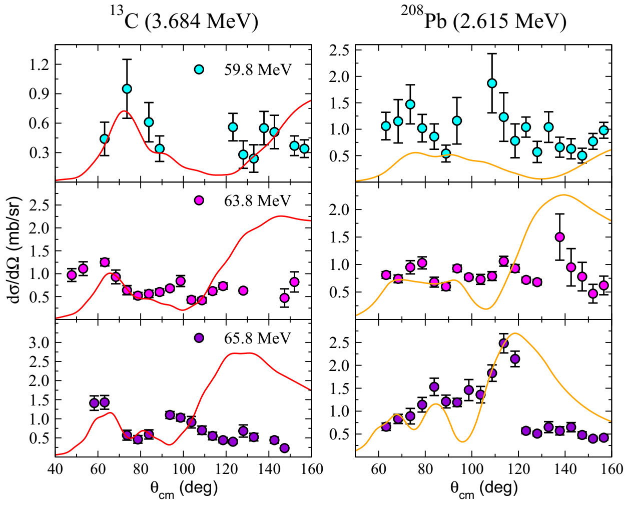

Fig. 6 Inelastic scattering angular distribution for the 3.684 MeV excited state of ^{13}C ($3/2^{-}$) and 2.615 MeV of ^{208}Pb (3^{-}) at bombarding energies E_{lab} = 59.8, 63.8 and 65.8 MeV, respectively. The solid curves are the CC calculations for both exited states

3.3 Coupling to 1n-stripping channel

As presented in the previous section, the inelastic excitations, while important, are not sufficient to reproduce the experimental data. This suggests that other reactions channels, such as transfer and/or breakup, may play important roles in the coupling scheme. The way to investigate the effect of transfer reactions is by performing a more complete coupling calculation by coupled reaction channel (CRC) calculations. Since

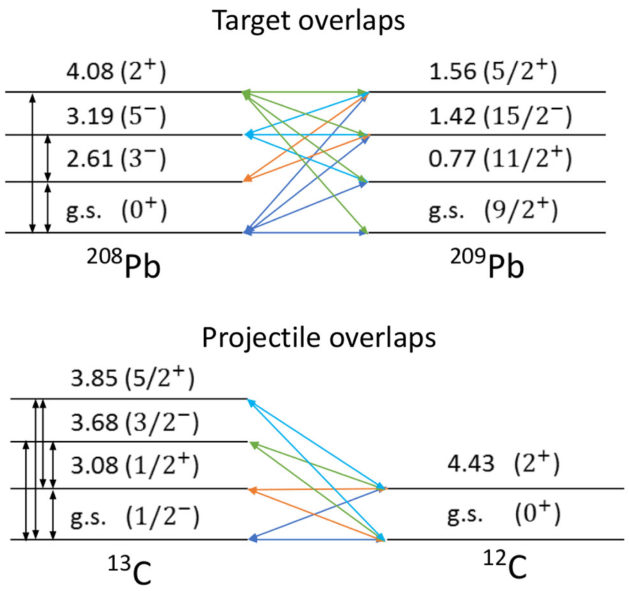

Fig. 7 Coupling scheme of projectile and target overlaps used in the CRC calculations for one neutron stripping

Table 3 Spectroscopy amplitudes, obtained with NuShellX code [32], used in the CRC calculations for one neutron stripping

Initial state	Final state	*nlj*	Spect. amp.
$^{13}\mathrm{C}_{g.s}$ $(1/2^-)$	$^{12}\mathrm{C}_{g.s}$ (0^+)	$1\mathrm{p}_{1/2}$	0.80
$^{13}\mathrm{C}_{g.s}$ $(1/2^-)$	$^{12}\mathrm{C}_{4.439}$ (2^+)	$1\mathrm{p}_{3/2}$	– 0.99
$^{13}\mathrm{C}_{3.08}$ $(1/2^+)$	$^{12}\mathrm{C}_{g.s}$ (0^+)	$2\mathrm{s}_{1/2}$	– 0.90
$^{13}\mathrm{C}_{3.08}$ $(1/2^+)$	$^{12}\mathrm{C}_{4.439}$ (2^+)	$1\mathrm{d}_{3/2}$	0.04
		$1\mathrm{d}_{5/2}$	– 0.31
$^{13}\mathrm{C}_{3.68}$ $(3/2^-)$	$^{12}\mathrm{C}_{g.s}$ (0^+)	$1\mathrm{p}_{3/2}$	0.36
$^{13}\mathrm{C}_{3.68}$ $(3/2^-)$	$^{12}\mathrm{C}_{4.439}$ (2^+)	$1\mathrm{p}_{1/2}$	0.82
		$1\mathrm{p}_{3/2}$	– 0.54
$^{13}\mathrm{C}_{3.85}$ $(5/2^+)$	$^{12}\mathrm{C}_{g.s}$ (0^+)	$1\mathrm{d}_{5/2}$	0.91
$^{13}\mathrm{C}_{3.85}$ $(5/2^+)$	$^{12}\mathrm{C}_{4.439}$ (2^+)	$2\mathrm{s}_{1/2}$	0.11
		$1\mathrm{d}_{3/2}$	– 0.06
		$1\mathrm{d}_{5/2}$	0.20

the neutron is the particle with the lowest binding energy in ^{13}C, with a separation energy of S_n = 4.946 MeV, we considered the neutron stripping reaction, ^{208}Pb (^{13}C,^{12}C)^{209}Pb with Q$_{value}$ = −1.0089 MeV, in the CRC method. For the real part of the potential for the entrance channel, we considered the double-folding São Paulo Potential, SPP2, with normalization factor N_R = 1.0. However, for the imaginary part, we used the same short-range potential from the previous CC calculation, to simulate the fusion absorption. The complex potential for the outgoing channel was entirely based on the double-folding São Paulo Potential, SPP2, with the real and imaginary normalization factors set to N_R = 1.0 and N_I = 0.78, respectively, because no couplings are explicitly considered in the outgoing partition.

The single-particle wave functions for the bound neutron in ^{13}C and ^{209}Pb nuclei were generated by considering Woods-Saxon form factors with reduced radii and diffuseness of 1.25 and 0.65 fm, respectively. The depths of the potentials were varied to reproduce the corresponding experimental binding energies for one neutron. The full complex remnant in the coupling matrix elements, with prior representation and non orthogonality corrections, was adopted in the full CRC calculations, also performed with the code FRESCO [31]. The overlap schemes for the 1*n*-stripping transfer reaction considered in the present CRC calculations, are shown in Fig. 7. For the projectile overlaps, the spectroscopic amplitudes were calculated by the shell model using the code NUSHELLX [32]. The *psdpn* model space and the *psdmod* effective phenomenological interaction [33] were used for the projectile overlaps. In this model, the ^{4}He is considered as a closed core and the $1p_{1/2}$, $1p_{3/2}$, $1d_{5/2}$, $1d_{3/2}$ and $2s_{1/2}$ were taken as valence subspace for neutrons. The obtained spectroscopic amplitudes for the selected states in the projectile are listed in Table 3. For the target overlaps, we consider the most important and representative states, adopting spectroscopic amplitudes equal to 1.0 for each *nlj* configuration.

The results of the finite-range CRC calculations, which includes the inelastic contribution and the contribution for the one neutron stripping are shown in Fig. 8 for each of the measured energies. A notable improvement in the description of the data can be observed, showing the importance of the 1*n*-stripping reaction to the coupling scheme. It is important to emphasize the complete absence of any imaginary potential at the interaction surface region. Also, this is a parameter-free calculation in the sense that there are no adjusted parameters. If a good description of the data is achieved, it is an indication that the correct number of channels has been included in the coupling matrix. In the present case, this effect resulted in a reduction of the intensity of the Fresnel peak, improving the agreement with the data and establishing the importance of the 1*n*-stripping reaction.

4 Conclusions

Full angular distributions for the elastic scattering of ^{13}C+^{208}Pb system at E$_{lab}$ = 59.8, 63.8 and 65.8 MeV, have been measured for the first time at energies close to the Coulomb barrier. The obtained angular distributions have been analyzed in terms of optical model (OM), coupled-channels (CC) and coupled reaction channel (CRC) calculations. The OM analysis has been used to derive the total reaction cross sections for this system. After an appropriate reduction, the obtained total reaction cross sections are

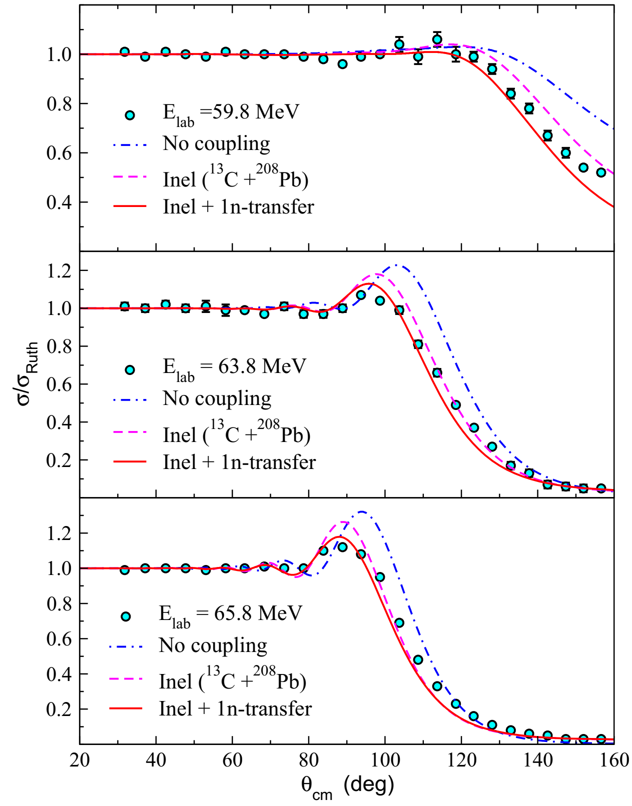

Fig. 8 Elastic scattering angular distribution for the ^{13}C+^{208}Pb at E_{lab} = 59.8, 63.8 and 65.8 MeV. The red solid curve are the full CRC calculations (taking into account the inelastic and $1n$-stripping contributions). The blue dashed-dotted curve represents the calculations without the couplings. The magenta dashed-dotted curve corresponds to the inelastic contribution from CC calculations

compared with values for some other light projectiles on the same target. The values are similar to those obtained for the ^{12}C isotope. The CC and CRC calculations have highlighted the importance of the dynamic effects in the description of the elastic data for this system. Specifically, nonelastic couplings of the excited states in ^{13}C and ^{208}Pb, and additional coupling to the $1n$-stripping reaction have been shown to be important. To complete the elastic scattering systematics for the carbon isotopes, data for ^{14}C+^{208}Pb system at close to the barrier energies would be welcome.

Acknowledgements The authors would like to thank the following foundations for financial support: CNPq (Grants 317451/2021-9, 403390/2021-4 and 131272/2022-5), Instituto Nacional de Ciências e Tecnologia - Física Nuclear e Aplicações (INCT/FNA) Proc. No. 464898/2014-5, FAPESP (process 2019/08344-7) and PNPD/CAPES (Process 88887.475459/2020-00). Argentinian authors acknowledge financial support from FONCyT (Fondo para la Investigación Científica y Tecnológica) Grant PICT-2019-3565. We also would like to thank the operators team at the Tandar Accelerator.

Data Availability Statement Data will be made available on reasonable request. [Authors' comment: Data can be provided in a table format on reasonable request].

Code Availability Statement This manuscript has no associated code/software. [Authors' comment: Code/Software sharing not applicable to this article as no code/software was generated or analysed during the current study.]

References

1. L.F. Canto, V. Guimarães, J. Lubian, M.S. Hussein, The total reaction cross section of heavy-ion reactions induced by stable and unstable exotic beams: the low-energy regime. Eur. Phys. J. A **56**, 281 (2020)
2. N. Keeley, N. Alamanos, K.W. Kemper, K. Rusek, Elastic scattering and reactions of light exotic beams. Prog. Part. Nucl. Phys. **63**(2), 396–447 (2009)
3. J.J. Kolata, V. Guimarães, E.F. Aguilera, Elastic scattering, fusion, and breakup of light exotic nuclei. Eur. Phys. J. A **52**(5), 123 (2016)
4. N. Keeley, Elastic scattering a hundred years on; what can it tell us? J. Phys: Conf. Ser. **381**(1), 012087 (2012)
5. N. Keeley, K.W. Kemper, K. Rusek, Strong coupling effects in near-barrier heavy-ion elastic scattering. Eur. Phys. J. A **50**(9), 145 (2023)
6. Y.Y. Yang, X. Liu, D.Y. Pang, D. Patel, R.F. Chen, J.S. Wang, P. Ma, J.B. Ma, S.L. Jin, Z. Bai, V. Guimarães, Q. Wang, W.H. Ma, F.F. Duan, Z.H. Gao, Y.C. Yu, Z.Y. Sun, Z.G. Hu, S.W. Xu, S.T. Wang, D. Yan, Y. Zhou, Y.H. Zhang, X.H. Zhou, H.S. Xu, G.Q. Xiao, W.L. Zhan, Elastic scattering of the proton drip line nuclei^{7}Be,^{8} B, and ^{9}C on a lead target atenergies around three times the coulomb barriers. Phys. Rev. C **98**, 044608 (2018)
7. Y.Y. Yang, J.S. Wang, Q. Wang, D.Y. Pang, J.B. Ma, M.R. Huang, P. Ma, S.L. Jin, J.L. Han, Z. Bai, L. Jin, J.B. Chen, Q. Hu, R. Wada, S. Mukherjee, Z.Y. Sun, R.F. Chen, X.Y. Zhang, Z.G. Hu, X.H. Yuan, S.W. Xu, S.Z. Chen, X.G. Lei, L.X. Liu, W.H. Ma, S.T. Wang, D. Yan, X.H. Zhang, M.H. Zhao, Y. Zhou, Y.J. Zhou, Z.Y. Guo, Y.H. Zhang, H.S. Xu, G.Q. Xiao, Quasi-elastic scattering of ^{10,11}C and^{10}B from a ^{nat}Pb target. Phys. Rev. C **90**, 014606 (2014)
8. C.C. Sahm, T. Murakami, J.G. Cramer, A.J. Lazzarini, D.D. Leach, D.R. Tieger, R.A. Loveman, W.G. Lynch, M.B. Tsang, J. Van der Plicht, Total reaction cross section for ^{12}C on ^{12}C, ^{40}Ca, ^{90}Zr, and^{208}Pb between 10 and 35 mev/nucleon. Phys. Rev. C **34**, 2165–2170 (1986)
9. J. Chauvin, D. Lebrun, A. Lounis, M. Buenerd, Low and intermediate energy nucleus-nucleus elastic scattering and the optical limit of glauber theory. Phys. Rev. C **28**, 1970–1974 (1983)
10. G. Yang, F.-F. Duan, K. Wang, Y.-Y. Yang, Z.-Y. Sun, V. Guimaraes, D.-Y. Pang, W.-D. Chen, L. Jin, S.-W. Xu, J.-B. Ma, P. Ma, Z. Bai, L.-H. Wang, Q. Liu, H.-J. Ong, B.-F. Lv, S. Guo, M.K. Raju, X.-H. Wang, R.-H. Li, Y.-H. Zhang, X.-H. Zhou, Z.-G. Hu, H.-S. Xu, Elastic scattering of ^{13}C and ^{14}C isotopes on a ^{208}Pb target at energies of approximately five times the coulomb barriers. Chin. Phys. C **48**(3), 034001 (2024)
11. R. Linares, M. Sinha, E.N. Cardozo, V. Guimarães, G.V. Rogachev, J. Hooker, E. Koshchiy, T. Ahn, C. Hunt, H. Jayatissa, S. Upadhyayula, B. Roeder, A. Saastomoinen, J. Lubian, M. Rodríguez-Gallardo, J. Casal, K.C.C. Pires, M. Assuncao, Y. Penionzhkevich, S. Lukyanov, Elastic scattering measurements for the^{10}C +^{208} Pb system at $E_{\rm lab}$ = 66 mev. Phys. Rev. C **103**, 044613 (2021)
12. J.D. Ovejas, A. Knyazev, I. Martel, O. Tengblad, M.J.G. Borge, J. Cederkall, N. Keeley, K. Rusek, C. García-Ramos, T. Pérez, L.A. Acosta, A.A. Arokiaraj, M. Babo, T. Cap, N. Ceylan, G. De Angelis, A. Di Pietro, J.P. Fernández, P. Figuera, L. Fraile, H. Fynbo, D. Galaviz, J.H. Jensen, B. Jonson, R. Kotak, T. Kurtukian, M. Madurga, G. Marquínez-Durán, M. Munch, A.K. Orduz, R. Honório, A. Pakou, L. Peralta, A. Perea, R. Raabe, M. Renaud, K. Riisager, A.M. Sánchez-Benítez, J. Sánchez-Segovia, O. Sgouros,

V. Soukeras, P. Teubig, S. Vinals, M. Wolinska-Cichocka, R. Wolski, J. Yang, Study of the scattering of ^{15}C at energies around the coulomb barrier. J. Phys: Conf. Ser. **1643**(1), 012095 (2020)

13. S. Santra, P. Singh, S. Kailas, A. Chatterjee, A. Shrivastava, K. Mahata, Coupled reaction channel analysis of elastic, inelastic, transfer, and fusion cross sections for ^{12}C +^{208} Pb. Phys. Rev. C **64**, 024602 (2001)
14. L.C. Chamon, B.V. Carlson, L.R. Gasques, São Paulo potential version 2 (spp2) and Brazilian nuclear potential (bnp). Comput. Phys. Commun. **267**, 108061 (2021)
15. V. Scarduelli, E. Crema, V. Guimarães, D. Abriola, A. Arazi, E. de Barbará, O.A. Capurro, M.A. Cardona, J. Gallardo, D. Hojman, G.V. Martí, A.J. Pacheco, D. Rodrígues, Y.Y. Yang, N.N. Deshmukh, B. Paes, J. Lubian, D.R. Mendes Junior, V. Morcelle, D.S. Monteiro, Elastic and inelastic scattering for the ^{10}B+^{58}Ni system at near-barrier energies. Phys. Rev. C **96**, 054610 (2017)
16. A. Arazi, J. Casal, M. Rodríguez-Gallardo, J.M. Arias, R. Lichtenthäler Filho, D. Abriola, O.A. Capurro, M.A. Cardona, P.F.F. Carnelli, E. de Barbará, J. Fernández Niello, J.M. Figueira, L. Fimiani, D. Hojman, G.V. Martí, D. Martínez Heimman, A.J. Pacheco, ^{9}Be +^{120} Sn scattering at near-barrier energies within a four-body model. Phys. Rev. C **97**, 044609 (2018)
17. F. Gollan, D. Abriola, A. Arazi, M.A. Cardona, E. de Barbará, D. Hojman, R.M. Id-Betan, G.V. Martí, A.J. Pacheco, D. Rodrigues, M. Togneri, Energy dependence of the optical potential of the weakly bound ^{9}Be projectile on the ^{197}Au target. Nucl. Phys. A **1000**, 121789 (2020)
18. F. Gollan, D. Abriola, A. Arazi, M.A. Cardona, E. de Barbará, D. Hojman, R.M. Id-Betan, G.V. Martí, A.J. Pacheco, D. Rodrigues, M. Togneri, Energy dependence of the optical potential of the weakly bound ^{9}Be projectile on the ^{197}Au target. Nucl. Phys. A **1000**, 121789 (2020)
19. J.M.B. Shorto, P.R.S. Gomes, J. Lubian, L.F. Canto, S. Mukherjee, L.C. Chamon, Reaction functions for weakly bound systems. Phys. Lett. B **678**(1), 77–81 (2009)
20. L.F. Canto, P.R.S. Gomes, J. Lubian, L.C. Chamon, E. Crema, Dynamic effects of breakup on fusion reactions of weakly bound nuclei. Nucl. Phys. A **821**(1), 51–71 (2009)
21. L.C. Chamon, B.V. Carlson, L.R. Gasques, D. Pereira, C. De Conti, M.A.G. Alvarez, M.S. Hussein, M.A. Cândido Ribeiro, E.S. Rossi, C.P. Silva, Toward a global description of the nucleus-nucleus interaction. Phys. Rev. C **66**, 014610 (2002)
22. C.Y. Wong, Interaction barrier in charged-particle nuclear reactions. Phys. Rev. Lett. **31**, 766–769 (1973)
23. L.F. Canto, P.R.S. Gomes, J. Lubian, L.C. Chamon, E. Crema, Disentangling static and dynamic effects of low breakup threshold in fusion reactions. J. Phys. G: Nucl. Part. Phys. **36**(1), 015109 (2008)
24. L.R. Gasques, L.C. Chamon, P.R.S. Gomes, J. Lubian, Comparison between heavy-ion reaction and fusion processes for hundreds of systems. Nucl. Phys. A **764**, 135–148 (2006)
25. L.F. Canto, R. Donangelo, M.S. Hussein, P. Lotti, J. Lubian, J. Rangel, Theoretical considerations about heavy-ion fusion in potential scattering. Phys. Rev. C **98**, 044617 (2018)
26. L.F. Canto, P.R.S. Gomes, J. Lubian, M.S. Hussein, P. Lotti, Assessing the adequacy of the bare optical potential in near-barrier fusion calculation. Eur. Phys. J. A **50**, 047601 (2014)
27. N.N. Deshmukh, V. Guimarães, E. Crema, D. Abriola, A. Arazi, E. de Barbará, O.A. Capurro, M.A. Cardona, J. Gallardo, D. Hojman, G.V. Martí, A.J. Pacheco, D. Rodrígues, Y.Y. Yang, A.N. Deshmukh, D.R. Mendes, V. Morcelle, V. Scarduelli, D.S. Monteiro, Elastic and inelastic scattering for the ^{11}B+^{58}Ni system: Target and projectile reorientation effects. Phys. Rev. C **92**, 054615 (2015)
28. A. Barbadoro, F. Pellegrini, G.F. Segato, L. Taffara, I. Gabrielli, M. Bruno, α-transfer contribution to ^{9}Be+^{13}C elastic and inelastic scattering. Phys. Rev. C **41**, 2425–2428 (1990)
29. Evaluated Nuclear Structure Data Files, National Nuclear Data Center, Brookhaven National Laboratory. https://www.nndc.bnl.gov/
30. Fresco code notes. http://www.fresco.org.uk/moro/frnotes.pdf
31. I.J. Thompson, Coupled reaction channels calculations in nuclear physics. Comput. Phys. Reports **7**(4), 167–212 (1988)
32. W. D. M. Rae. NushellX—large scale shell model calculations on your PC (2008)
33. Yutaka Utsuno, Satoshi Chiba, Multiparticle-multihole states around ^{16}O and correlation-energy effect on the shell gap. Phys. Rev. C **83**, 021301 (2011)